Hybrid Beamforming Design for Communication-Centric ISAC

Leonardo Leyva, Daniel Castanheira, Adão Silva, and Atílio Gameiro

***Abstract*— The integration of communication and radio-sensing functionalities on the same network has attracted attention recently, a paradigm designated as integrated sensing and communication (ISAC). This paper addresses the problem of fully-connected hybrid beamforming design for a multi-user and multi-beam ISAC scenario. Previous methods of fully-connected hybrid beamforming usually deal with this problem in two steps. First, the fully digital beamformer is obtained and then the hybrid beamformer is selected to minimize the distance to the fully digital counterpart. However, this approach may exhibit some drawbacks since the original communication and radio-sensing requirements may not be preserved. In contrast in this work, the fully-connected hybrid beamforming is designed to ensure that communication and radio-sensing-related constraints are always fulfilled. The considered optimization criterion is the maximization of the weighted sum rate subject to power budget and radio-sensing constraints. To address this problem, we propose a novel and convergent iterative alternate optimization algorithm to design the hybrid beamforming matrices that satisfy the criteria for both communication and radio-sensing. The simulation results have shown that the performance is close to the fully digital precoder and outperforms other previous fully-connected hybrid beamforming design methods for ISAC.**

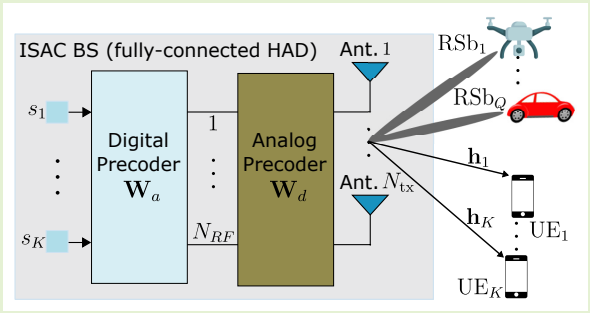

***Index Terms*— Integrated sensing and communication; fully-connected hybrid beamforming; multi-user communication; radio-sensing; multi-beam steering, iterative alternate optimization.**

I. Introduction

Wireless communication and radio-sensing systems have been historically developed in parallel as independent radio systems, with regulators ensuring interference-free operation [1]–[6]. However, the spectrum scarcity in specific geographic regions and frequency bands motivated the research into more efficient coexistence approaches like opportunistic spectrum access, and projection-based techniques [1], [7], [8]. Although those techniques partially relieve the spectrum scarcity issue, their implementation requires inter-system collaboration, and dedicated hardware since communication and radio-sensing are still separated systems.

More recently, the integration of radio-sensing and communication functionalities on the same platform has been proposed, known as integrated sensing and communication (ISAC) [4]–[6], [9]. ISAC solves the spectrum scarcity problem but also uses the resources efficiently (hardware, network infrastructure, etc.), and even pursues mutual benefits. Therefore, in addition to solving the spectrum shortage, ISAC has been identified as a key technology to enable a range of use cases in next-generation wireless systems. In particular, ISAC has been proposed to support future WiFi [10] and 6G [11] applications, such as indoor fall detection, unmanned mobility, and industry 4.0 [12]. Nonetheless, to enable a radio-sensing dimension towards 6G, it is essential to further research key technologies from the ISAC viewpoint, such as beamforming. Beamforming for ISAC systems refers to the spatial signal processing used in the design of precoding matrices to simultaneously provide communication and radio-sensing applications efficiently. Consequently, this area has evolved into a timely subject, leading to several contributions about fully digital (FD) [13]–[15], and hybrid analog-digital (HAD) [6], [12], [16]–[19] beamforming design methods for ISAC scenarios.

In [13], the authors designed the precoding matrices that formulate an appropriate radio-sensing probing beampattern while guaranteeing that the signal-to-interference-plus-noise ratio (SINR) of multiple communication users and total power budget constraints. The results demonstrated that the ISAC transmission yields better overall performance than the coexistence scenario, where antennas are separated to deliver com-

This paragraph of the first footnote will contain the date on which you submitted your paper for review. This work has received funding from the FCT - Fundação para a Ciência e a Tecnologia under the PhD Research Studentships 2022.12379.BD and REVOLUTION project 2022.08005.PTDC, and from FCT/MCTES through national funds and when applicable co-funded EU funds under the project UIDB/50008/2020-UIDP/50008/2020. Additionally, this work has received funding from the European Union's Horizon Europe research under the Smart Networks and Services Joint Undertaking (SNS JU) project 6GMUSICAL, grant agreement No. 101139176.

Leonardo Leyva, Daniel Castanheira, Adão Silva and Atílio Gameiro are with the Instituto de Telecomunicações, and with Departamento de Electrónica, Telecomunicações e Informática, Universidade de Aveiro, 3810-164, Aveiro, Portugal. (E-mails: leoleval@av.it.pt, dcastanheira@av.it.pt, asilva@av.it.pt, amg@ua.pt).

munication and radio-sensing operations separately. Similarly, [14] designed a dual-function precoder that minimizes a radio-sensing loss function subject to SINR and total power constraints in a multi-user scenario. Unlike [13], the paper studied jointly precoded individual communication and radio-sensing waveforms, which increases the degree of freedom (DoF) of the radio-sensing waveform but generates interference in the communication receivers. Previously discussed methods are radio-sensing centric, as a radio-sensing metric is optimized, such as matching a desired radio-sensing beampattern, while meeting communication constraints. More recently, the authors of [15] considered both, radio-sensing and communication centric designs, respectively. In the communication-centric solution, the sum-rate with multiple user-equipments (UE) is maximized, subject to the signal-clutter-noise ratio (SCNR) and power budget. In [15], the authors consider a monostatic scenario, but the self-interference is neglected in the SCNR. Also, the proposed algorithm is limited to formulating a single beam for target detection, which further limits the radio-sensing possibilities.

The contributions mentioned above focused on the design of a fully digital precoder, which requires a radio-frequency (RF) chain for antenna elements. However, deploying fully digital precoders in transmitters with many antennas leads to high hardware costs and power consumption. Hence, similar to what happened in wireless communication and radar, the ISAC research community has recently revealed interest in HAD beamforming design methods [6], [12], [16]–[19]. Table I classifies the cited publications based on key elements like the HAD architecture, the ISAC scenario, the primary functionality (communication, radio-sensing, and weighted approach), and whether a two-stage approach was used (i.e., FD precoder approximation).

The initial contribution in this area concerns the investigation conducted by the authors of [16]. The authors proposed a partially-connected hybrid beamforming design for a single-user MIMO (SU-MIMO) and multi-beam ISAC scenario. More specifically, a MIMO BS communicates with a multiple-antenna UE, while formulating radio-sensing beams toward several directions. They derived the HAD beamforming matrices that minimize the weighted sum of the Euclidean distances to the desired communication and radio-sensing precoders (previously obtained), subject to a power budget constraint. This initial contribution was restricted to the partially-connected architecture and SU-MIMO ISAC scenario. In [6], a single-user and multi-beam ISAC scenario is also contemplated, but a fully-connected HAD beamforming design is derived. The design approximates a zero-forcing (ZF) precoder, but the columns of the analog precoder are first set to the corresponding radio-sensing steering vectors. Therefore, this approach reduces degrees of freedom (DoF) of the analog beamformer to an alphabet of steering vectors. More recently, the authors of [12] considered the fully-connected hybrid beamforming design problem for a multi-user and multi-beam ISAC scenario. The devised algorithm does not depend on approximation to the FD precoder but solves the HAD beamforming matrices through the optimization of a weighted sum between communication and radio-sensing metrics, subject to a power budget constraint. More specifically, the weighted sum between the spectral efficiency (SE), and the spatial spectrum matching error (SSME) is considered as optimization objective. Due to the high complexity of the weighted optimization problem, the authors proposed an iterative algorithm based on the consensus alternating direction method of multipliers (CADMM). Likewise, [17] addressed the fully-connected hybrid beamforming design problem by considering the weighted sum between the SE and SINR for communication and radio-sensing, respectively. Similarly to [12], the authors employed a CADMM algorithm to obtain a solution for the problem. Although [12], [17] investigated the fully-connected hybrid beamforming design problem for multi-user and multi-beam ISAC, different weights lead to different objectives. Therefore, to meet a given communication/radio-sensing metric, the correct weights must be selected, which may be difficult [20]. To handle this issue one of the metrics (radio-sensing or communication) must be considered as a constraint. Compared to the weighted objective method this approach has a simpler objective but more involved constraints [20]. In [18], the authors followed this approach and devised an algorithm for the HAD beamforming design from a radio-sensing centric point of view. Namely, it was considered the minimization of the angle estimation Cramér-Rao bound (CRB) while ensuring that the SINR values of communication users are satisfied. However, this contribution was restricted to a partially-connected architecture. In contrast, [19] investigated the fully-connected hybrid beamforming design for a radio-sensing centric ISAC scenario. The method minimizes the Euclidean distance to an optimal radio-sensing transmit beampattern subject to SINR constraints of communication users and power budget. Contrarily to the partially-connected architecture, the power budget constraint cannot be removed from the analog part design bringing further complexity to the problem to be solved. Therefore, the authors proposed a two-stage optimization method. The first phase obtains the fully-digital precoder that matches a desired transmitted beampattern subject to SINR constraints. Then, a second stage yields the HAD beamforming matrices that approximate the previously determined fully digital precoder. The main drawback of [19] is that it can not guarantee that the constraints

TABLE I: Resume of relevant features about HAD beamforming design for ISAC systems.

Contribution	HAD arquitecture	ISAC scenario	Primary functionality	Two-stage approach
[16]	partially-connected	single-user/multi-beam	weighted communication/radio-sensing	yes
[6]	fully-connected	single-user/multi-beam	weighted communication/radio-sensing	yes
[12], [17]	fully-connected	multi-user/multi-beam	weighted communication/radio-sensing	no
[18]	partially-connected	multi-user/multi-beam	radio-sensing centric	no
[19]	fully-connected	multi-user/multi-beam	radio-sensing centric	yes

considered in the first phase are preserved when resolving the HAD matrices in the second phase. Therefore even if the weighted objective approach [12], [17] is not considered, at the end, the original communication constraints in [19] may still not be fulfilled. Motivated by the aforementioned drawback, our work aims to design the fully-connected hybrid beamforming matrices that always guarantee the fulfillment of the set of constraints. Contrary to the revised literature, we derived a solution from a communication-centric perspective. Besides, the proposed algorithm does not approximate an FD precoder.

This work considers the problem of fully-connected hybrid beamforming design for a multi-user and multi-beam ISAC scenario. A multi-antenna BS simultaneously transmits data towards several single-antenna UEs while scanning a desired geographic area by steering radio-sensing probing beams. We propose a novel algorithm for the design of the hybrid beamforming matrices under a communication-centric objective. The main contributions of this work include:

- Design of fully-connected hybrid beamforming for multi-user and multi-beam ISAC scenarios. Unlike [12, 17, 19], the proposed HAD design is communication-centric and guarantees that the examined set of radio-sensing constraints is always satisfied.
- Reformulation of the considered ISAC non-convex optimization constrained problem into a more manageable form by leveraging the equivalence between weighted sum-rate maximization and weighted-sum mean-squared-error (WMMSE) minimization, first developed for communication in [22].
- Proposal of a novel convergent and iterative alternate optimization algorithm. For ISAC, the WMMSE formulation has no closed-form solution and the hybrid structure introduces non-convex constraints into the problem. Furthermore, as mentioned, the power budget constraint brings further complexity to fully-connected architecture.

The results demonstrate improved communication performance with lower complexity and zero outage probability (probability of not satisfying radio sensing requirements) when compared with previous methods recently proposed in the literature. Specifically, a performance close to the fully digital implementation is achieved with a moderate number of RF chains.

The remainder of this paper is organized as follows. Section II describes the transmitted signal, communication receiver and radio-sensing models. Section III presents the problem formulation, the more tractable equivalent optimization problem and details the alternate optimization algorithm. In Section IV, the proposed algorithm is evaluated and compared to other algorithms proposed in the literature. Finally, Section V outlines the main conclusions of this paper.

Notation: Complex scalars are represented by normal font, i.e., a, vectors and matrices are denoted by bold lowercase and bold uppercase letters, respectively, i.e., $\mathbf{a}$, and $\mathbf{A}$. $\mathbb{E}$ stands as the expectation operator, $\mathbb{C}$ and $\mathbb{R}$ denote the set of complex and real numbers, respectively. Besides, $[\cdot]^T$, $[\cdot]^*$, and $[\cdot]^H$, indicate the transpose, conjugate and Hermitian transpose operations, respectively. Finally, $\mathrm{diag}(\cdot)$ denotes the diagonal matrix of a vector, $\Re(\cdot)$ represents the real part of a complex scalar, $||\cdot||_F$ denotes the Frobenius norm and $\mathbf{A}\otimes\mathbf{B}$ is the Kronecker product between $\mathbf{A}$ and $\mathbf{B}$. The vector $\mathbf{e}_k$ denotes the kth column of the identity matrix.

II. System Model

This work considers the scenario described in Fig. 1. The transmitter is an ISAC base station ($\mathrm{BS_{tx}}$) equipped with a uniform linear array (ULA) holding N_{tx} antenna elements. The $\mathrm{BS_{tx}}$ jointly serves K single-antenna user equipment (UE) and steers Q radio-sensing probing beams (RSb) pointing towards ϕ_q directions for target detection. The channel between the $\mathrm{BS_{tx}}$ and UEs can be either line-of-sight (LoS) or non-line-of-sight (NLoS), while the targets are assumed to have LoS with the $\mathrm{BS_{tx}}$ and are illuminated by the RSbs.

In Fig. 1 the radio-sensing signal processing, namely target detection and estimation of targets parameters, is done in a bistatic receiver (designated as $\mathrm{BS_{rx}}$) or a central unit (CU) as proposed in [5]. The reason to consider a bistatic topology is related to the self-interference issues inherent to the monostatic topologies. In this arrangement, the communication signals can be used for sensing as either the CU or $\mathrm{BS_{rx}}$ knows the communication signals transmitted by the $\mathrm{BS_{tx}}$. In the following, it is assumed that the channel state information (CSI) is known by $\mathrm{BS_{tx}}$. The CSI may be acquired by utilizing pilot signals, where conventional techniques like minimum mean squared error (MMSE) and least-squares (LS) [21] can be used. Considering FDD, the channel is estimated at the UE, and the parameters are transmitted through an appropriate channel to the BStx. If TDD is considered, the BStx may exploit the uplink-downlink reciprocity to estimate the uplink channel and then use it in the downlink slot. Also, to guarantee that objects in a given geographical area are illuminated with enough power, $\mathrm{BS_{tx}}$ knows the required power of the transmit beampattern in the direction of the radio-sensing probing beams.

A. Transmitted Signal Model

We consider downlink transmission for an MU-MIMO system operating in the mmWave band. In order to minimize power consumption, the $\mathrm{BS_{tx}}$ uses an HAD beamformer with N_{RF} radio-frequency (RF) chains. It is assumed that the data symbols used for communications are also used for radio-sensing purposes. Consequently, the transmitted signal can be expressed as

$$\begin{aligned}\mathbf{x} =& \mathbf{W}_a\mathbf{W}_d\mathbf{s}\\ =& \mathbf{W}_a\sum_{k=1}^{K}\mathbf{w}_{d,k}s_k\end{aligned} \tag{1}$$

where $\mathbf{s} = [s_1,\cdots,s_K]^T \in \mathbb{C}^K$ denotes the transmitted data stream, $\mathbf{W}_d = [\mathbf{w}_{d,1},\cdots,\mathbf{w}_{d,K}] \in \mathbb{C}^{N_{RF}\times K}$ represents the digital precoder, for which $\mathbf{w}_{d,k}$ is the precoder vector intended for the kth UE, and $\mathbf{W}_a \in \mathbb{C}^{N_{\mathrm{tx}}\times N_{RF}}$ is the analog precoder.

The transmitter model assumes that the entries of $\mathbf{s}$ are independent with unitary power, $\mathbb{E}[\mathbf{s}\mathbf{s}^H] = \mathbf{I}_K$. The model also assumes a fully connected HAD structure, where each RF

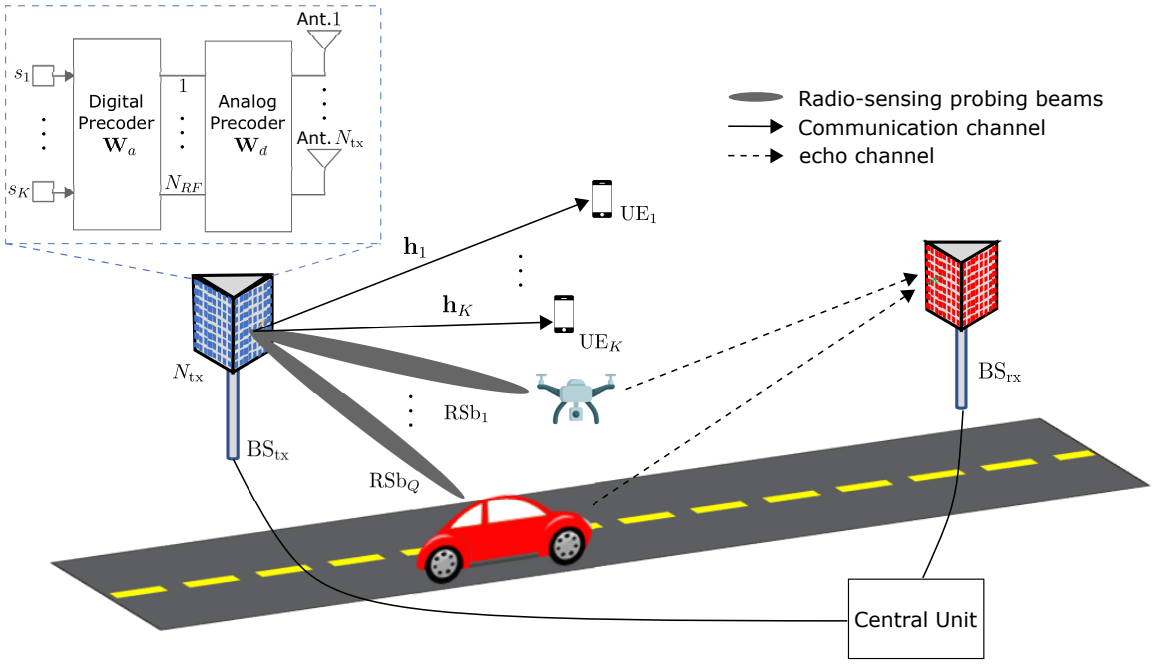

Fig. 1: Illustration of the considered ISAC system. The BS_{tx} jointly serves K single-antenna UEs, while steering Q RSbs. Both BSs are interconnected via a backhaul to a central unit. The radio-sensing signal processing is performed between BS_{rx} and the CU.

chain is connected to all antenna elements via phase shifters. As a result, each element of $\mathbf{W}_a$ has a constant modulus (CM), given by $(\sqrt{N_{\text{tx}}N_{RF}})^{-1}$. Furthermore, the available power budget of the ISAC-BS is constrained by P_T as

$$||\mathbf{W}_a\mathbf{W}_d||_F^2 \leq P_T. \tag{2}$$

B. Communication Receiver Model

After passing through the channel, assumed for simplicity to be a narrowband block-fading propagation channel [23], the transmitted signal (1) is received by the kth UE. Thus, the received signal y_k can be represented as

$$\begin{aligned} y_k &= \mathbf{h}_k^H\mathbf{x} + n_k \\ &= \mathbf{h}_k^H\mathbf{W}_a\mathbf{w}_{d,k}s_k + \mathbf{h}_k^H\mathbf{W}_a\sum_{i=1,i\neq k}^{K}\mathbf{w}_{d,i}s_i + n_k \end{aligned} \tag{3}$$

where the first term is the desired signal, the second term describes the inter-user interference, and n_k is the receiver noise, which is additive white Gaussian noise (AWGN) with zero mean and variance σ_k^2. The vector $\mathbf{h}_k \in \mathbb{C}^{N_{\text{tx}}}$ represents the channel between the kth single-antenna UE and the ISAC-BS. As refered, the communication channel $\mathbf{h}_k \in \mathbb{C}^{N_{\text{tx}}}$ can be modeled as a narrowband block-fading propagation channel [23]. Formally,

$$\mathbf{h}_k = \frac{1}{\sqrt{H}}\sum_{h=1}^{H}\alpha_h\mathbf{a}_{N_{\text{tx}}}(\theta_h) \tag{4}$$

where H is the number of paths, α_h stands as the complex gain of the hth path, and the vector $\mathbf{a}_{N_{\text{tx}}}(\theta_h)$ represents the transmit array response vector in the direction of θ_h. The array response vector for an ULA consisting of N antenna elements can be expressed as

$$\mathbf{a}_N(\theta) = \left[1,\ e^{j\frac{2\pi}{\lambda}d\sin(\theta)},\ \cdots,\ e^{j\frac{2\pi}{\lambda}d(N-1)\sin(\theta)}\right]^T \tag{5}$$

where d and λ are the inter-element spacing and the signal wavelength, respectively.

Considering (3), the SINR of the kth UE is given by,

$$\text{SINR}_k = \frac{|\mathbf{h}_k^H\mathbf{W}_a\mathbf{w}_{d,k}|^2}{\sum_{i\neq k}|\mathbf{h}_k^H\mathbf{W}_a\mathbf{w}_{d,i}|^2 + \sigma_k^2}. \tag{6}$$

The rate of the kth UE can be obtained as

$$R_k = \log\left(1 + \text{SINR}_k\right). \tag{7}$$

C. Radio-sensing Model

For radio-sensing purposes, the ISAC-BS directs Q radio-sensing probing beams toward $\phi_q\ \forall q$. Therefore, the transmitted signal in the direction of the qth radio-sensing probing beam is given by,

$$\begin{aligned} g_q &= \mathbf{g}_q^H\mathbf{x} \\ &= \mathbf{g}_q^H\mathbf{W}_a\sum_{k=1}^{K}\mathbf{w}_{d,k}s_k, \end{aligned} \tag{8}$$

where $\mathbf{g}_q \in \mathbb{C}^{N_{\text{tx}}}$ represents the transmit array response vector (5) in the direction ϕ_q (i.e., $\mathbf{g}_q = \mathbf{a}_{N_{\text{tx}}}(\phi_q)$). Hence, the average power of the transmit beampattern in the direction ϕ_q can be represented by [24],

$$\text{G}(\phi_q) = \mathbf{g}_q^H\mathbf{R}\mathbf{g}_q \tag{9}$$

$$= \sum_{k=1}^{K}|\mathbf{g}_q^H\mathbf{W}_a\mathbf{w}_{d,k}|^2. \tag{10}$$

where $\mathbf{R}$ is the covariance matrix of the transmitted signal (1), which follows from

$$\mathbf{R} = \mathbb{E}[\mathbf{x}\mathbf{x}^H] = \mathbf{W}_a \mathbf{W}_d \mathbf{W}_d^H \mathbf{W}_a^H. \tag{11}$$

III. Hybrid Beamforming Design

This section proposes a novel algorithm aimed at designing the optimal fully-connected hybrid beamforming matrices. The problem is formulated as the weighted sum-rate maximization [25], subject to total power budget and radio-sensing constraints. The considered optimization problem is non-convex and difficult to solve [22], [25]. Hence, it is reformulated into a more tractable form by using the equivalence between the maximization of the weighted sum-rate and the WMMSE minimization optimization problem [22]. However, in contrast to the scenario of [22], for which a closed-form solution exists, the hybrid architecture and radio-sensing constraints considered in our problem prevent the existence of such a closed-form solution. Therefore, we develop a novel iterative alternate optimization algorithm for designing the fully-connected hybrid beamforming matrices.

A. Problem Formulation

The problem under consideration involves designing the hybrid beamforming matrices to maximize the weighted sum-rate of the downlink communication system while satisfying the total power budget and a transmit beampattern gain in the direction of the radio-sensing probing beams. Consequently, the problem can be formulated as,

$$\max_{\mathbf{W}_a, \mathbf{W}_d} \sum_k \alpha_k R_k \tag{12a}$$

$$\text{s.t.} \quad ||\mathbf{W}_a \mathbf{W}_d||_F^2 \leq P_T \tag{12b}$$

$$\mathrm{G}(\phi_q) \geq \Delta_q, \ \forall q \tag{12c}$$

$$\mathbf{W}_a \in \mathcal{A} \tag{12d}$$

where α_k is a weight that determines the priority assigned to the kth UE, Δ_q represents the threshold that determines the minimum required power of the transmit beampattern in the direction of the qth radio-sensing probing beam. The set $\mathcal{A}$ describes the feasible set of analog beamforming matrices with CM.

B. WMMSE-Based Equivalent Optimization Problem

The optimization problem (12) exhibits a non-convex structure. This is because of the non-convex nature of both the objective function and the sets represented by constraints (12c) and (12d). Using the equivalence between maximization of the weighted sum-rate and minimization of the WMMSE [22], the problem (12) can be equivalently formulated as

$$\min_{\mathbf{W}_a, \mathbf{W}_d, \omega_k, u_k} \sum_k \alpha_k \omega_k e_k - \log(\omega_k)$$

$$\text{s.t.} \quad ||\mathbf{W}_a \mathbf{W}_d||_F^2 \leq P_T \tag{13}$$

$$\mathrm{G}(\phi_q) \geq \Delta_q, \ \forall q$$

$$\mathbf{W}_a \in \mathcal{A}$$

where ω_k and u_k are the kth UE weight and equalizer, and e_k is the mean squared error (MSE) between the soft decision $\hat{s}_k$ and the transmitted signal s_k. The MSE is given by,

$$\begin{aligned} e_k =& \mathbb{E}[(\hat{s}_k - s_k)(\hat{s}_k - s_k)^H] \\ =& |1 - u_k^* \mathbf{h}_k^H \mathbf{W}_a \mathbf{w}_{d,k}|^2 + \sum_{i \neq k} |u_k^* \mathbf{h}_k^H \mathbf{W}_a \mathbf{w}_{d,i}|^2 \\ &+ |u_k|^2 \sigma_{n_k}^2 \end{aligned} \tag{14}$$

where, the soft decision $\hat{s}_k$ follows from $\hat{s}_k = u_k^* y_k$, and y_k is the received signal at the kth UE, see (3).

The previous establishes that minimizing the WMMSE (13) is equivalent to maximizing the weighted sum-rate (12). However, solving (13) is simpler due to its quadratic objective function. To solve (13) an alternate optimization method could be used, where ω_k and u_k have closed-form optimal solutions. The optimal solution for u_k is given by the MMSE receiver,

$$u_k^\circ = \mathrm{j}_k^{-1} \mathbf{h}_k^H \mathbf{W}_a \mathbf{w}_{d,k} \tag{15}$$

where $\mathrm{j}_k = \sum_{i=1}^K |\mathbf{h}_k^H \mathbf{W}_a \mathbf{w}_{d,i}|^2 + \sigma_{n_k}^2$ is the variance of the received signal at the kth UE, while ω_k optimal solution is $\omega_k^\circ = e_k^{-1}$ [22]. However, due to the non-convex nature of the CM and radio-sensing constraints, to our best knowledge, it is not possible to find a closed-form solution for the hybrid beamforming matrices. Consequently, an iterative alternate algorithm has been developed to obtain $\mathbf{W}_a$ and $\mathbf{W}_d$, under the assumption that the remaining variables remain fixed.

C. Iterative Alternate Algorithm for Hybrid Beamforming Design

This section provides a comprehensive description of the proposed iterative alternate algorithm for obtaining $\mathbf{W}_a$ and $\mathbf{W}_d$. As mentioned earlier, (12c) and (12d) define non-convex sets, making (13) a challenging problem to solve. To address the non-convexity of (12c), it is replaced with a more restrictive and convex constraints. On the other hand, the non-convexity of (12d) is handled by resorting to several transformations (i.e., upper-bound function, projection, equivalent problems, etc.) that result in a version of (13) where a solution for $\mathbf{W}_a$ and $\mathbf{W}_d$ can be found.

Under the alternate minimization framework, as previously mentioned, $\mathbf{W}_a$ and $\mathbf{W}_d$ can be solved over (13), when $\omega_k = \omega_k^\circ$ and $u_k = u_k^\circ$ are fixed. Thus, by substituting (14) into (13), we can reframe the optimization problem as follows,

$$\min_{\mathbf{W}_a, \mathbf{W}_d} ||\mathbf{\Phi}^{1/2}(\mathbf{I} - \mathbf{\Psi} \mathbf{H}_{\mathrm{UE}}^H \mathbf{W}_a \mathbf{W}_d)||_F^2 \tag{16a}$$

$$\text{s.t.} \quad ||\mathbf{W}_a \mathbf{W}_d||_F^2 \leq P_T \tag{16b}$$

$$\frac{1}{\sqrt{K}} \sum_k \Re(\mathbf{g}_q^H \mathbf{W}_a \mathbf{W}_d \mathbf{e}_k) = \Delta_q^{1/2} \quad \forall q \tag{16c}$$

$$\mathbf{W}_a \in \mathcal{A} \tag{16d}$$

where $\mathbf{\Phi} = \mathrm{diag}\{\alpha_1 \omega_1, \cdots, \alpha_K \omega_K\}$, $\mathbf{\Psi} = \mathrm{diag}\{u_1^*, \cdots, u_K^*\}$, and $\mathbf{H}_{\mathrm{UE}} = [\mathbf{h}_1, \cdots, \mathbf{h}_K]$. The objective function in (16a) is the same as in (13) but in matrix form, using (14). To handle constraint (12c), which is non-convex, it was replaced by (16c). This new constraint is convex but it

is more restrictive since the set defined by this constraint is a subset of (12c), accordingly to proposition 1.

Proposition 1: Let us define $\mathcal{B} = \{\mathbf{W}_a, \mathbf{W}_d : (12c)\}$ and $\hat{\mathcal{B}} = \{\mathbf{W}_a, \mathbf{W}_d : (16c)\}$, then $\hat{\mathcal{B}} \subseteq \mathcal{B}$.

Proof: Sets $\mathcal{B}$ and $\hat{\mathcal{B}}$ define the points satisfying constraints (12c) and (16c). As $\|\mathbf{x}\|$ is a convex function, it can be lower-bounded by the linear function $\Re(\mathbf{x}_0^H\mathbf{x}/\|\mathbf{x}_0\|)$, which is valid for any $\mathbf{x}_0$. For $\mathbf{x}_0 = \mathbf{1}$ follows the inequality $\|\mathbf{x}\| \geq \Re(\mathbf{1}^T\mathbf{x}/\|\mathbf{1}\|) = 1/\sqrt{K}\sum_k \Re(\mathbf{x}^H\mathbf{e}_k)$. If $\mathbf{x} = (\mathbf{g}_q^H\mathbf{W}_a\mathbf{W}_d)^H$ then proposition 1 follows. ∎

From previous proposition follows that the optimal value of the original problem is lower than the new one, but the solution always fulfills the original constraint.

The previous optimization can be reformulated by defining the Lagrangian function

$$\begin{aligned}\mathcal{L}(\mathbf{W}_a, \mathbf{W}_d, \mu_q) =& ||\mathbf{\Phi}^{1/2}(\mathbf{I} - \mathbf{\Psi}\mathbf{H}_{\mathrm{UE}}^H\mathbf{W}_a\mathbf{W}_d)||_F^2 \\ &- \sum_q \mu_q \left(\Re\{\mathrm{tr}(\mathbf{G}_q^H\mathbf{W}_a\mathbf{W}_d)\} - \Delta_q^{1/2}\right)\end{aligned} \tag{17}$$

that includes the radio-sensing constraints. The reformulated problem is

$$\begin{aligned}\min_{\mathbf{W}_a,\mathbf{W}_d}\ & \mathcal{L}(\mathbf{W}_a, \mathbf{W}_d, \mu_q) \\ \text{s.t.}\quad & ||\mathbf{W}_a\mathbf{W}_d||_F^2 \leq P_T \\ & \mathbf{W}_a \in \mathcal{A}\end{aligned} \tag{18}$$

where μ_q are the Lagrangian multipliers, and $\mathbf{G}_q = \frac{1}{\sqrt{K}}\mathbf{1}_{1\times K} \otimes \mathbf{g}_q$ is the radio-sensing steering vector in matrix form. The relation between the previous problems is specified in the next proposition.

Proposition 2: The problems (16) and (18) are equivalent when Lagrangian multipliers μ_q are selected such that (16c) is satisfied.

Proof: Let $\mu_q = \mu_q^*$ be selected such constraint (16c) is respected, then $\mathcal{L}(\mathbf{W}_a, \mathbf{W}_d, \mu_q^*)$ is identical to (16) objective function. Therefore, the problems' solution will be identical, since both the objective function and remaining constraints are the same. ∎

The structure of (17) makes (18) still a difficult problem. Hence, we define an upper-bound function of (17), which is derived in Appendix A. Therefore, the upper-bounded optimization problem can be recast as

$$\begin{aligned}\min_{\mathbf{W}_a,\mathbf{W}_d}\ & ||\mathbf{W}_a\mathbf{W}_d - \hat{\mathbf{W}}_0||_F^2 \\ \text{s.t.}\quad & ||\mathbf{W}_a\mathbf{W}_d||_F^2 \leq P_T \\ & \mathbf{W}_a \in \mathcal{A}\end{aligned} \tag{19}$$

where

$$\hat{\mathbf{W}}_0 = \mathbf{W}_{a,0}\mathbf{W}_{d,0} - \alpha\nabla\mathcal{L}(\mathbf{W}_{a,0}, \mathbf{W}_{d,0}, \mu_q^*), \tag{20}$$

$\mathbf{W}_{a,0}$, and $\mathbf{W}_{d,0}$ denote the previous iteration analog and digital precoders. Also, $\alpha = 1/\lambda_{\max}(\mathbf{H}_{\mathcal{L}})$ denotes the inverse of the maximum eigenvalue of the Hessian matrix of (17), where $\mathbf{H}_{\mathcal{L}} = \tilde{\mathbf{H}}_{\mathrm{UE}}^H\tilde{\mathbf{H}}_{\mathrm{UE}}$. Additionally, $\nabla\mathcal{L}(\mathbf{W}_{a,0}, \mathbf{W}_{d,0})$ represents the gradient of (17) when evaluated at $(\mathbf{W}_{a,0}, \mathbf{W}_{d,0}, \mu_q)$, which is given by

$$\begin{aligned}\nabla\mathcal{L}(\mathbf{W}_{a,0}\mathbf{W}_{d,0}, \mu_q) =& \tilde{\mathbf{H}}_{\mathrm{UE}}^H\tilde{\mathbf{H}}_{\mathrm{UE}}\mathbf{W}_{a,0}\mathbf{W}_{d,0} \\ &- \tilde{\mathbf{H}}_{\mathrm{UE}}^H\mathbf{\Phi}^{1/2} - \frac{1}{2}\sum_q \mu_q\mathbf{G}_q.\end{aligned} \tag{21}$$

where $\tilde{\mathbf{H}}_{\mathrm{UE}} = \mathbf{\Phi}^{1/2}\mathbf{\Psi}\mathbf{H}_{\mathrm{UE}}^H$ represents an equivalent channel. Note that the upper-bound function is a distance that measures how far the hybrid precoder is to a given precoder objective. The precoder objective changes from iteration to iteration and can be thought of as the hybrid precoder obtained when moving along the steepest descent direction of $\mathcal{L}$. Therefore, in contrast to the method proposed in [19], which considers a similar problem but with a fixed precoder objective, here the precoder objective is modified over the iterations in order to obtain a solution for the original problem.

The power constraint when paired with the CM constraint makes the solution of (19) difficult. Therefore, the power constraint is included in the objective function of (19), remaining only the CM constraint as stated in theorem 1.

Theorem 1: Let $\mathbf{W}_a^\circ$, $\mathbf{W}_d^\circ$ be the optimal solution of (19) and define $\overline{\mathbf{W}}_a^\circ$, $\overline{\mathbf{W}}_d^\circ$ as the optimal solution to,

$$\begin{aligned}\min_{\mathbf{W}_a,\mathbf{W}_d}\ & ||\mathbf{W}_a\mathbf{W}_d - \hat{\mathbf{W}}_0||_F^2 + ||\mathbf{W}_a\mathbf{W}_d||_F^2 \\ \text{s.t.}\quad & \mathbf{W}_a \in \mathcal{A},\end{aligned} \tag{22}$$

then the optimal analog solutions are identical in both problems, $\mathbf{W}_a^\circ = \overline{\mathbf{W}}_a^\circ$, and the digital solution of (19) is a projection of the solution of (22) into the set defined by the power constraint, $\mathbf{W}_d^\circ = \mathcal{P}(\overline{\mathbf{W}}_a^\circ, 2\overline{\mathbf{W}}_d^\circ)$, with the projection operator defined as

$$\mathcal{P}(\mathbf{W}_a, \mathbf{W}_d) = \begin{cases}\mathbf{W}_d, & \|\mathbf{W}_a\mathbf{W}_d\|_F^2 \leq P_T \\ \frac{\sqrt{P_T}}{\|\mathbf{W}_a\mathbf{W}_d\|_F}\mathbf{W}_d, & \text{otherwise.}\end{cases} \tag{23}$$

Proof: see Appendix B ∎

Theorem 1 states that problems (19) and (22) are equivalent in the sense that optimization over $\mathbf{W}_a$ is identical in both problems. Notice that $\mathbf{W}_a$ solution is easier to obtain using (22) than (19) since there is no power constraint. Therefore, the solutions for $\mathbf{W}_a$ and $\mathbf{W}_d$ can be obtained by alternating over (22) and projecting $\mathbf{W}_d$ using (23). The following subsections detail how the solutions for $\mathbf{W}_a$ and $\mathbf{W}_d$ are obtained.

1) Analog Beamforming Design: The analog precoder $\mathbf{W}_a$ is optimized by minimizing an upper-bound of (22) objective function. The detailed derivation of the upper-bound is provided in Appendix C. Consequently, (22) can be reformulated as follows,

$$\begin{aligned}\max_{\mathbf{W}_a}\ & \Re(\mathrm{tr}((\mathbf{W}_{a,0} - \beta\nabla\mathrm{f}(\mathbf{W}_{a,0}))^H\mathbf{W}_a)) \\ \text{s.t. } & \mathbf{W}_a \in \mathcal{A}\end{aligned} \tag{24}$$

where the gradient is given by,

$$\nabla\mathrm{f}(\mathbf{W}_{a,0}) = (2\mathbf{W}_{a,0}\mathbf{W}_{d,0} - \hat{\mathbf{W}}_0)\mathbf{W}_{d,0}^H \tag{25}$$

and $\beta = 1/\lambda_{\max}(\mathbf{H}_{\mathrm{f}(\mathbf{W}_a)})$ with $\mathbf{H}_{\mathrm{f}(\mathbf{W}_a)} = 2\mathbf{W}_{d,0}\mathbf{W}_{d,0}^H$. From (24), we can observe that the optimal $\mathbf{W}_a$ is given by,

$$\mathbf{W}_a = \frac{1}{\sqrt{N_{\mathrm{tx}}N_{RF}}}\mathcal{R}(\mathbf{W}_{a,0} - \beta\nabla\mathrm{f}(\mathbf{W}_{a,0})). \tag{26}$$

where $\mathcal{R}$ is a retraction over the complex circle manifold defined as,

$$\mathcal{R}(w) = \frac{w}{|w|} \tag{27}$$

where w is a complex scalar. For matrices, the retraction is applied to each entry. Note that in (26) the analog hybrid precoder part is obtained by moving first along the steepest descent direction of (24) objective, and then projecting the result along the CM constraint to make the solution feasible.

2) Digital Beamforming Design: The optimal $\mathbf{W}_d$ results from solving (22), but considering that $\mathbf{W}_a$ is fixed to $\mathbf{W}_{a,0}$. Hence, (22) can be reformulated as

$$\min_{\mathbf{W}_d} ||\mathbf{W}_{a,0}\mathbf{W}_d - \hat{\mathbf{W}}_0||_F^2 + ||\mathbf{W}_{a,0}\mathbf{W}_d||_F^2. \tag{28}$$

The solution of the above problem is given by,

$$\overline{\mathbf{W}}_d = \frac{1}{2}(\mathbf{W}_{a,0}^H\mathbf{W}_{a,0})^{-1}\mathbf{W}_{a,0}^H\hat{\mathbf{W}}_0. \tag{29}$$

According to theorem (1) the power constraint is satisfied through the projection defined in (23) as

$$\mathbf{W}_d = \mathcal{P}(\mathbf{W}_{a,0}, 2\overline{\mathbf{W}}_d). \tag{30}$$

All steps of the derivation ensure that the new objective majorizes the previous optimizations objective. Therefore, it is ensured that the proposed method strictly improves performance over the iterations. As the objective function value is lower bounded by zero it always converges to a fixed value [26].

The proposed WMMSE-based iterative alternate optimization algorithm is summarized by Algorithm 1. Notice that the value of μ_q^* (see proposition 2) used in step 5 may be obtained through a multi-dimensional numerical search method.

Algorithm 1: WMMSE-based Iterative Alternate Optimization Algorithm for Hybrid Beamforming Design.

Result: $\mathbf{W}_a$, $\mathbf{W}_d$
Input: P_T; ϵ; $\mathbf{H}_{\text{UE}}$; $\{\mathbf{g}_q\}$; $\{\Delta_q\}$; I_0; I_1; σ^2
1. Randomly initialize $\mathbf{W}_a \in \mathcal{C}^{N_{\text{tx}} \times N_{RF}}$ such that each entry presents CM with value $\sqrt{N_{\text{tx}}N_{RF}}^{-1}$;
2. Randomly initialize $\mathbf{W}_d \in \mathcal{C}^{N_{RF} \times K}$ such that $||\mathbf{W}_a\mathbf{W}_d||_F^2 = P_T$;
for $l1 = 1 : I_0$ **do**
  3. $u_k^\circ = \mathrm{j}_k^{-1}\mathbf{h}_k^H\mathbf{W}_a\mathbf{w}_{d,k}\ \forall k$;
  4. $\omega_k^\circ = (1 - u_k^{\circ *}\mathbf{h}_k^H\mathbf{W}_a\mathbf{w}_{d,k})^{-1}\ \forall k$;
  for $l2 = 1 : I_1$ **do**
    5. $\hat{\mathbf{W}}_0 = \mathbf{W}_{a,0}\mathbf{W}_{d,0} - \alpha\nabla\mathcal{L}(\mathbf{W}_{a,0}, \mathbf{W}_{d,0}, \mu_q^*)$;
    6. $\overline{\mathbf{W}}_d = \frac{1}{2}(\mathbf{W}_{a,0}^H\mathbf{W}_{a,0})^{-1}\mathbf{W}_{a,0}^H\hat{\mathbf{W}}_0$;
    7. $\mathbf{W}_a = \frac{1}{\sqrt{N_{\text{tx}}N_{RF}}}\mathcal{R}(\mathbf{W}_{a,0} - \beta\nabla \mathrm{f}(\mathbf{W}_{a,0}))$;
    8. $\mathbf{W}_d = \mathcal{P}(\mathbf{W}_{a,0}, 2\overline{\mathbf{W}}_d)$, where $\mathbf{W}_{a,0}$ follows from step 7;
    9. Update $\mathbf{W}_a^\circ$ and $\mathbf{W}_d^\circ$;
    10. Compute sum-rate according to (12)
  end
end

D. Computational Complexity Analysis

The primary computational complexity of the proposed algorithm lies in designing the hybrid beamforming matrices, with particular emphasis on computing (20), (26), and (29). Specifically, solving (20) entails a complexity of $\mathcal{O}(N_{\text{tx}}^3 + 2N_{\text{tx}}^2K + 2N_{\text{tx}}N_{RF}K)$, which can be approximated by $\mathcal{O}(N_{\text{tx}}^3)$. This complexity stems from operations such as singular value decomposition and matrix multiplications. Solving (26) involves a complexity of $\mathcal{O}(N_{RF}^3 + 2N_{\text{tx}}N_{RF}K)$, which simplifies to $\mathcal{O}(N_{RF}^3)$, this complixity is due to singular value decomposition and matrix multiplication. Solving (29) exhibits a complexity of $\mathcal{O}(N_{RF}^3 + 2N_{\text{tx}}^2N_{RF} + N_{\text{tx}}N_{RF}K)$, primarily attributed to matrix inversion.

In summary, the overall complexity of the proposed algorithm is $\mathcal{O}(I_{\text{ter}}(N_{\text{tx}}^3 + N_{RF}^3 + 2N_{\text{tx}}^2N_{RF}))$, where $I_{\text{ter}} = I_0I_1$, I_0 and I_1 set the number of iterations for the WMMSE-based equivalent problem (13), and the iterative alternate algorithm used for the design of $\mathbf{W}_a$ and $\mathbf{W}_d$ (16), respectively. Notice that the computational complexity is similar to the algorithm proposed in [12].

IV. Numerical Results

This section validates the proposed WMMSE-based iterative alternate optimization algorithm, referred to as ItAlHAD. The ItAlHAD algorithm is compared with the fully digital precoder, the two stage alternating minimization algorithm introduced in [19], referred to as TwoS-AltMin, and the method in [12] designated as CADMM. To ensure fairness in the comparisons, the hybrid beamforming obtained through the TwoS-AltMin approach involves approximating a fully digital precoder generated by the ItAlHAD algorithm, setting $N_{RF} = N_{\text{tx}}$. On the other hand, the method in [12] resolves the hybrid beamforming through the CADMM algorithm. The simulations were carried out on a physical server equipped with an Intel Xeon E5645 CPU and 24 GB of RAM. The operating system used is Windows 10, and the simulation software employed is MATLAB 2022a.

The following results consider that the BS_{tx} is equipped with an ULA holding $N_{\text{tx}} = 32$ elements spaced by $\lambda/2$, and the signal-to-noise ratio (SNR) is set to 30 dB. The communication channel is characterized by a mmWave geometric model, as described in (4). Here, θ_h follows a uniform distribution ranging from $(-\pi/2,\ \pi/2]$, and α_h follows a Gaussian distribution with a mean of zero and unit variance. Additionally and unless otherwise specified, the number of scattering paths is set to 10. The power budget of the hybrid beamforming is set to $P_T = 1$. Besides, it is considered that the communication and radio-sensing channels are normalized, i.e., $\mathbb{E}[\mathbf{h}_k^H\mathbf{h}_k] = \|\mathbf{g}_q\|^2 = 1$. Consequently, the gain of transmit beampattern in the direction of the radio-sensing probing beams (9) can only take values between $(0, 1]$. In decibel, the power of the transmit beampattern is computed according to

$$\mathrm{G}(\phi_q)_{\text{dBi}} = 10\log(N_{\text{tx}}\mathrm{G}_q). \tag{31}$$

The remainder of this section provides an analysis of the convergence behavior of the proposed algorithm. This is

followed by a study of how the radio-sensing constraint value impacts the transmit beampattern and the achieved sum-rate. Subsequently, the outage probability (the probability of not satisfying the radio-sensing constraint) is evaluated. Finally, the sum-rate is assessed by considering the impact of the number of RF chains and SNR value.

The convergence of the sum-rate (see (12b)) is illustrated in Fig. 2. The scenario under consideration involves $K = 4$ UEs and $Q = 1$ radio-sensing probing beam directed towards $10°$. Additionally, two configurations are examined, namely, fully-connected HAD architectures with $N_{RF} \in \{4, 8\}$, respectively. Fig. 2 presents the convergence obtained over 1000 iterations. Nevertheless, simulations indicate that the algorithm reached a stable value considerably earlier. It can be verified,

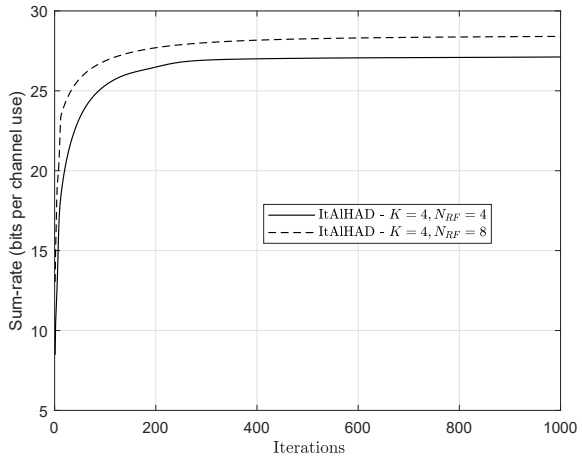

Fig. 2: The convergence of the weighted sum-rate obtained by the proposed ItAlHAD algorithm for fully-connected HAD architectures with $N_{RF} \in \{4, 8\}$, respectively.

from Fig. 2, that the algorithm strictly improves performance with the number of iterations. This is valid for both scenarios as expected from the algorithm design as explained in section III-C. Namely, the algorithm converges with approximately 250 iterations for both configurations (i.e., $N_{RF} \in \{4, 8\}$). Also, it can be noticed that the configuration with $N_{RF} = 6$ converges to a greater sum-rate, which is due to the two additional RF chains.

Fig. 3 illustrates the transmitted beampattern for a scenario with $K = 4$ UEs (for ease of exposition both the communication and radio-sensing channels are LoS), and $Q = 2$ radio-sensing probing beams are considered. The UEs are positioned at angles $-50°, -20°, 25°, 45°$, while the radio-sensing probing beams point at $-10°$ and $10°$. In Fig. 3, we consider that the radio-sensing constraint is the same for both radio-sensing beams, that is $\Delta_1 = \Delta_2$. The result in Fig. 3 reveals a trade-off between the power of the transmit beampattern in the direction of the radio-sensing probing beams and the UEs. It is clear that as the radio-sensing constraints Δ_1 and Δ_2 values increase, the power in the direction of the UEs decreases, which directly influences the sum-rate. Therefore, the following result investigates this trade-off and compares it with the fully digital, TwoS-AltMin and CADMM algorithms.

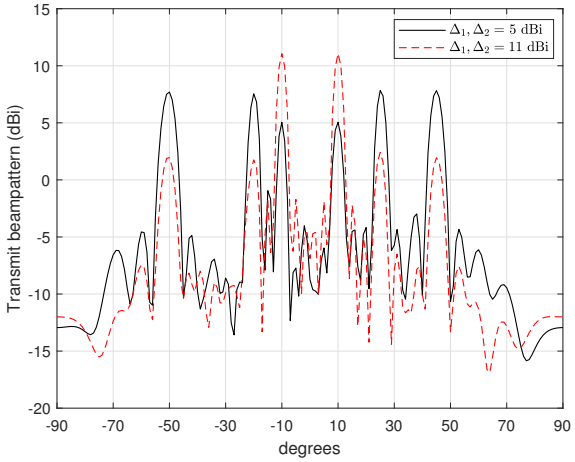

Fig. 3: The resulting transmit beampattern for a scenario with $K = 4$ UEs and $Q = 2$ radio-sensing probing beams, obtained for a hybrid architecture with $N_{\text{tx}} = 32$ and $N_{RF} = 4$.

Fig. 4 displays the trade-off between the mean sum-rate obtained for $K = 4$ UEs and the constraint Δ_1 for $Q = 1$ radio-sensing probing beams. The mean sum-rate is obtained for values of Δ_1 ranging from 0.1 to 0.9, in decibels from 5 to 14.6 dBi. Different HAD configurations are evaluated, namely $N_{RF} \in \{4, 6\}$. For ease of presentation, the comparison with the fully digital precoder, and TwoS-AltMin algorithm is shown in Fig. 4a, while the comparison with the CADMM algorithm is displayed in Fig. 4b. The parameter η in Fig. 4b weights the radar and communications metrics. A higher η value indicates a better radar performance [12]. The results depicted in Fig. 4a demonstrate that the ItAlHAD algorithm outperforms the TwoS-AltMin algorithm for both HAD configurations, $N_{RF} \in \{4, 6\}$. These findings show the superior efficiency of the proposed algorithm. Specifically, with only 4 RF chains, the ItAlHAD algorithm achieves better performance compared to TwoS-AltMin with 6 RF chains. This occurs because the TwoS-AltMin algorithm fails to deliver an accurate approximation of the fully digital precoder when $N_{RF} < 2K$. In addition, we got the result for a HAD configuration with $N_{RF} = 8$, but for clarity, the curve was omitted in Fig. 4a. For $N_{RF} = 8$, the ItAltMin and TwoS-AltMin algorithms exhibit a similar performance, closely approaching that of the fully digital solution. In contrast, Fig. 4b illustrates that the CADMM algorithm achieves a higher mean sum-rate than the ItAlHAD algorithm. However, as it will be further detailed, this is because to the high probability that the constraint Δ_1 may not be fulfilled by the CADMM algorithm. This occurs because the method in [12] does not consider Δ_1 as constraint but rather minimizes a weighted communication/radio-sensing objective function. For comparison, we have set different values to the weight η, but the simulations have shown that meeting a specific radio-sensing constraint is quite difficult. Besides, the ItAlHAD and CADMM methods present similar computational complexity (see section III.D, and [12]), but our algorithm always fulfill the set of constraints, in contrast to the CADMM.

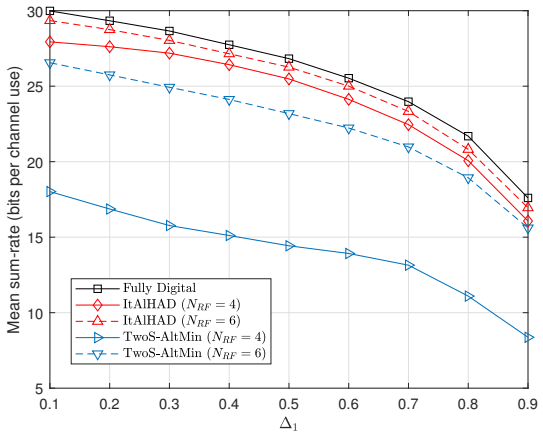

(a)

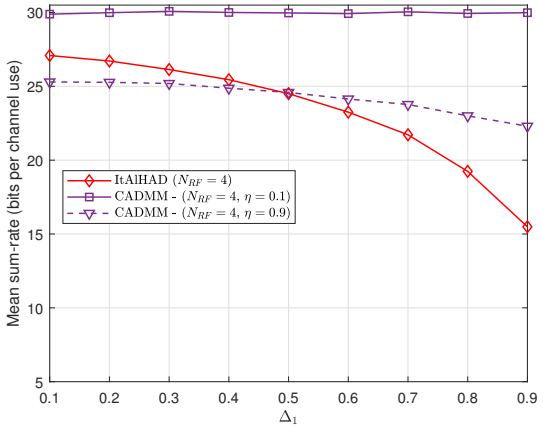

(b)

Fig. 4: The trade-off between the mean sum-rate and the constraint Δ_1 obtained for a scenario with $K=4$ and $Q=1$: (a) comparison with fully digital, and TwoS-AltMin algorithm for $N_{RF} \in \{4,6\}$, (b) comparison with CADMM algorithm for $N_{RF}=4$ and $\eta \in \{0.1, 0.9\}$.

Notice that from Fig. 4, the compliance of the constraint (12c) can not be examined. Hence, Fig. 5 illustrates the cumulative distribution function (CDF) of the power of the transmit beampattern in the direction of $Q=1$ (i.e., $\mathrm{G}(\phi_1)$), given by (9), for a radio-sensing constraint value of $\Delta_1 = 0.3$ and $N_{RF}=4$. More specifically, Fig. 5 displays the CDFs obtained for the proposed ItAltHAD, TwoS-AltMin and CADMM algorithms. Fig. 5 shows that the proposed ItAlHAD algorithm consistently fulfills the constraint Δ_1. This remains valid for any HAD arquitecture. In contrast, it can be seen that both the TwoS-AltMin and CADMM algorithms do not satisfy the set constraint value Δ_1, which is more critical for the CADMM algorithm. This means that the outage probability (probability of not satisfying the radio-sensing requirements) of the TwoS-AltMin, and the CADMM algorithms are not zero, in contrast to the proposed method. For this specific scenario, the outage probability of the TwoS-AltMin is around 2%, while the CADMM reported 30%, which is high, and

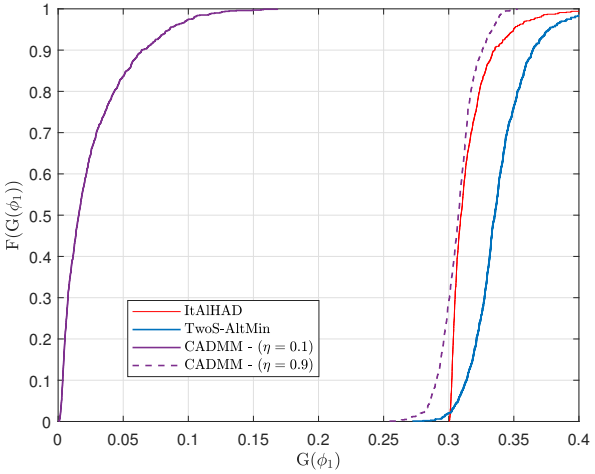

Fig. 5: The CDF of $\mathrm{G}(\phi_1)$ obtained for $\Delta_1=0.3$, $N_{RF}=4$, $K=4$ and $Q=1$.

higher than the TwoS-AltMin. Also, the simulations showed that the CADMM may even report an outage probability of 100% for specific scenarios. More specifically, the outage probability is highly dependent on the η value selected. The lower the η the better the mean-sum rate performance but the outage probability degrades significantly, meaning that the radar-requested performance target could not be fulfilled. Therefore, in the following we constraint the comparison of the proposed ItAltHAD algorithm with the TwoS-AltMin approach. Denoting the outage probability of the radio-sensing constraint as $\mathrm{P}(\mathrm{G}(\phi_1)) \leq \Delta_1$, table II summarizes the outage probability obtained for the TwoS-AltMin algorithm for different HAD configurations and values of $\Delta_1 = 0.1, 0.3, 0.5$. The

TABLE II: The outage probability $\mathrm{P}(\mathrm{G}(\phi_1)) \leq \Delta_1$ obtained for the TwoS-AltMin algorithm.

Δ_1	$N_{RF}=4$	$N_{RF}=6$	$N_{RF}=8$
0.1	20%	15%	4.3%
0.3	2%	10%	4.9%
0.5	0	4.6%	4.6%

results in table II showcase that the TwoS-AltMin algorithm cannot guarantee that the constraint (12c), considered in the design of the fully digital precoder, is preserved.

Fig. 6 investigates the mean sum-rate for different HAD configurations (number of active RF chains N_{RF}). There are assessed two scenarios, where the scheduled UEs are set to $K \in \{4,6\}$. For both scenarios $Q=1$ with $\Delta_1 = 0.3$. Fig. 6 demonstrates that the proposed ItAlHAD algorithm clearly outperforms the TwoS-AltMin algorithm for scenarios where N_{RF} is less than or equal to twice number of UEs, i.e., $N_{RF} \leq 2K$. Otherwise, both algorithm reports a similar performance in terms of mean sum-rate. The gap for $K = N_{RF}$ is around 10 bits per channel use between the two methods. The proposed method achieves a performance close to the full-digital method with a much lower number of RF chains, leading to improved energy efficiency.

The result in Fig. 7 analyses the mean sum-rate of the

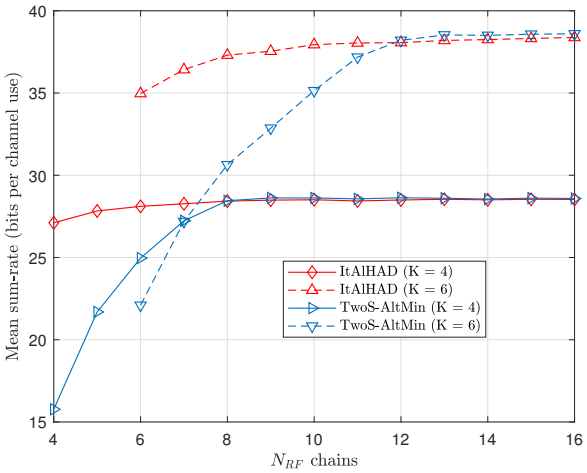

Fig. 6: The mean sum-rate with respect to N_{RF} for the proposed ItAlHAD, and TwoS-AltMin algorithms.

proposed ItAlHAD and TwoS-AltMin algorithms versus the SNR for $K = 8$, $Q = 1$ and $N_{RF} = 8$. By observing Fig.

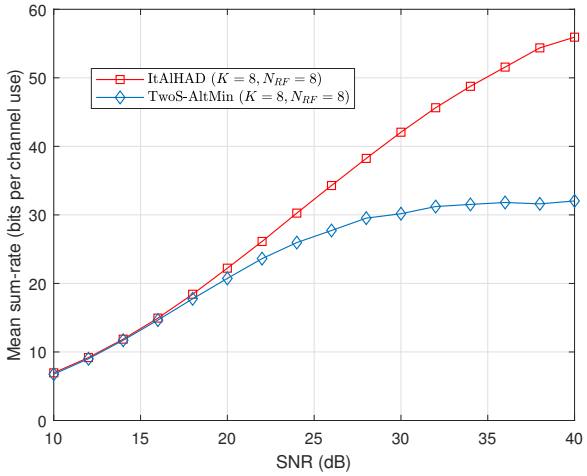

Fig. 7: The mean sum-rate versus the SNR values.

7, it becomes evident that the proposed algorithm achieves superior performance compared to the TwoS-AltMin algorithm when the SNR exceeds 20 dB. However, in the low SNR range, both methods exhibit similar performance. Additionally, it is worth noting that the ItAlHAD algorithm demonstrates a linear relationship with the SNR, whereas the TwoS-AltMin algorithm appears to exhibit a saturation behavior in the high SNR regime.

V. Conclusions

This paper assessed the problem of fully-connected hybrid beamforming design for an MU-MIMO and multi-target/beam ISAC scenario. The problem was formulated as the maximization of the weighted sum-rate subject to the total power budget and radio-sensing constraints. The problem is non-convex and therefore difficult to solve. Hence, it was reformulated into a more manageable equivalent problem by leveraging the WMMSE problem, but the hybrid architecture still precluded a closed-form solution. Therefore, we proposed an iterative alternate optimization algorithm to design the optimal fully-connected hybrid beamforming matrices. Simulation results assessed the performance of the proposed ItAlHAD algorithm in terms of mean sum-rate, and transmitted power in the direction of the radio-sensing probing beams. Besides, the performance of the ItAlHAD algorithm was compared with a fully-digital precoder, the TwoS-AltMin and the CADMM algorithms in the literature. The results showed that the performance of the proposed ItAlHAD algorithm is close to the full digital precoder and outperforms the TwoS-AltMin, and the CADMM algorithms recently proposed in the literature. The proposed method yields satisfactory results even when few RF chains are available, leading to an energy-efficient solution.

Appendix I
Derivation of Upper-bound Function for (17)

In this appendix we derive an upper-bound for (17). Let $\mathbf{W} = \mathbf{W}_a\mathbf{W}_d$, then (17) can be rewritten as

$$\begin{aligned} \mathrm{f}(\mathbf{W}) =& ||\mathbf{\Phi}^{1/2}(\mathbf{I} - \mathbf{\Psi}\mathbf{H}_{\mathrm{UE}}^H\mathbf{W}_a\mathbf{W}_d)||_F^2 \\ &- \sum_q \mu_q \left(\Re\{\mathrm{tr}(\mathbf{G}_q^H\mathbf{W}_a\mathbf{W}_d)\} - \Delta_q^{1/2}\right) \end{aligned} \tag{32}$$

Using the second-order Taylor polynomial, $\mathrm{f}(\mathbf{W})$ can be expressed as,

$$\begin{aligned} \mathrm{f}(\mathbf{W}) =& \mathrm{f}(\mathbf{W}_0) + 2\Re(\mathrm{tr}(\nabla^H\mathrm{f}(\mathbf{W}_0)(\mathbf{W} - \mathbf{W}_0))) \\ &+ \mathrm{tr}((\mathbf{W} - \mathbf{W}_0)^H\mathbf{H}_{\mathrm{f}(\mathbf{W})}(\mathbf{W} - \mathbf{W}_0)) \end{aligned} \tag{33}$$

where $\nabla\mathrm{f}(\mathbf{W})$ and $\mathbf{H}_{\mathrm{f}(\mathbf{W})}$ are the gradient and the Hessian of (32). Notice that (32) is a second-order function, then the Hessian is a constant.

The upper-bound function $\mathrm{g}(\mathbf{W})$ can be obtained as,

$$\begin{aligned} \mathrm{g}(\mathbf{W}) =& \mathrm{f}(\mathbf{W}_0) + 2\Re(\mathrm{tr}(\nabla^H\mathrm{f}(\mathbf{W}_0)(\mathbf{W} - \mathbf{W}_0))) \\ &+ \alpha^{-1}||\mathbf{W} - \mathbf{W}_0||_F^2 \end{aligned} \tag{34}$$

where $\alpha = 1/\lambda_{\max}(\mathbf{H}_{\mathrm{f}(\mathbf{W})})$ with $\lambda_{\max}(\cdot)$ denoting the maximum eigenvalue, which ensures $\mathrm{f}(\mathbf{W}) \leq \mathrm{g}(\mathbf{W})$. Notice that $\mathrm{g}(\mathbf{W}_0) = \mathrm{f}(\mathbf{W}_0)$. The equation in (34) can be rewritten as,

$$\mathrm{g}(\mathbf{W}) = \alpha^{-1}||\mathbf{W} - (\mathbf{W}_0 - \alpha\nabla\mathrm{f}(\mathbf{W}_0))||_F^2 + c \tag{35}$$

where c is a constant and $\nabla\mathrm{f}(\mathbf{W}_0)$ is given by

$$\nabla\mathrm{f}(\mathbf{W}_0) = \tilde{\mathbf{H}}_{\mathrm{UE}}^H\tilde{\mathbf{H}}_{\mathrm{UE}}\mathbf{W}_0 - \tilde{\mathbf{H}}_{\mathrm{UE}}^H\mathbf{\Phi}^{1/2} - \frac{1}{2}\sum_q \mu_q\mathbf{G}_q \tag{36}$$

and $\tilde{\mathbf{H}}_{\mathrm{UE}} = \mathbf{\Phi}^{1/2}\mathbf{\Psi}\mathbf{H}_{\mathrm{UE}}^H$ defines the equivalent channel matrix. Finally, we have that

$$\mathrm{f}(\mathbf{W}) \leq \alpha^{-1}||\mathbf{W} - (\mathbf{W}_0 - \alpha\nabla\mathrm{f}(\mathbf{W}_0))||_F^2 + c \tag{37}$$

which finalizes the proof.

APPENDIX II
PROOF OF THE EQUIVALENCE BETWEEN (19) AND (22)

This appendix demonstrates the equivalence between the optimization problems (19) and (22). Let us solve (19) for $\mathbf{W}_d$ as,

$$\begin{aligned} &\min_{\mathbf{W}_d} ||\mathbf{W}_a\mathbf{W}_d - \hat{\mathbf{W}}_0||_F^2 \\ &\text{s.t.} \quad ||\mathbf{W}_a\mathbf{W}_d||_F^2 \leq P_T. \end{aligned} \tag{38}$$

Note that (38) is a least square (LS) constrained optimization problem, for which the solution is given by,

$$\mathbf{W}_d^{\circ} = \mathcal{P}(\mathbf{W}_a, (\mathbf{W}_a^H\mathbf{W}_a)^{-1}\mathbf{W}_a^H\hat{\mathbf{W}}_0) \tag{39}$$

where the projection operator $\mathcal{P}(\cdot)$ is defined in (23). From (39)

$$\mathbf{W}_a\mathbf{W}_d^{\circ} = \begin{cases} \mathbf{Q}\hat{\mathbf{W}}_0, & ||\mathbf{W}_a\mathbf{W}_d||_F^2 \leq P_T \\ \sqrt{P_T}\frac{\mathbf{Q}\hat{\mathbf{W}}_0}{||\mathbf{Q}\hat{\mathbf{W}}_0||_F}, & \text{otherwise} \end{cases} \tag{40}$$

where $\mathbf{Q} = \mathbf{W}_a(\mathbf{W}_a^H\mathbf{W}_a)^{-1}\mathbf{W}_a^H$. Hence, substituting (39) into the objective function in (38), we have

$$\mathrm{f}(\mathbf{W}_a) = \begin{cases} \|\mathbf{Q}\hat{\mathbf{W}}_0 - \hat{\mathbf{W}}_0\|_F^2, & ||\mathbf{W}_a\mathbf{W}_d||_F^2 \leq P_T \\ \|\sqrt{P_T}\frac{\mathbf{Q}\hat{\mathbf{W}}_0}{||\mathbf{Q}\hat{\mathbf{W}}_0||_F} - \hat{\mathbf{W}}_0\|_F^2, & \text{otherwise.} \end{cases} \tag{41}$$

Similarly, we solve the related problem (22) for $\mathbf{W}_d$,

$$\min_{\mathbf{W}_d} ||\mathbf{W}_a\mathbf{W}_d - \hat{\mathbf{W}}_0||_F^2 + ||\mathbf{W}_a\mathbf{W}_d||_F^2 \tag{42}$$

for which, the solution is

$$\overline{\mathbf{W}}_d^{\circ} = \frac{1}{2}(\mathbf{W}_a^H\mathbf{W}_a)^{-1}\mathbf{W}_a^H\hat{\mathbf{W}}_0. \tag{43}$$

which is identical to (39) if multiplied by 2 and normalized by operator $\mathcal{P}(\cdot)$, i.e., $\mathbf{W}_d^{\circ} = \mathcal{P}(\mathbf{W}_a, 2\overline{\mathbf{W}}_d^{\circ})$. Substituting (43) into the objective function of (42), we get

$$\mathrm{g}(\mathbf{W}_a) = \frac{1}{2}||\mathbf{Q}\hat{\mathbf{W}}_0 - \hat{\mathbf{W}}_0||_F^2 + c \tag{44}$$

where $c = \frac{3}{4}\mathrm{tr}(\hat{\mathbf{W}}_0\hat{\mathbf{W}}_0^H)$ is a constant. From (41) and (44), it can be seen directly that optimizing over $\mathbf{W}_a$ is identical in both problems when the constraint $\|\mathbf{W}_a\mathbf{W}_d\|_F^2 \leq P_T$ is fulfilled in (41). However, this equivalence can not be seen directly from previous equations. Therefore, we recast $\mathrm{f}(\mathbf{W}_a)$ as,

$$\mathrm{f}(\mathbf{W}_a) = c_1 - 2\sqrt{P_T}\|\mathbf{Q}\hat{\mathbf{W}}_0^H\|_F \tag{45}$$

while $\mathrm{g}(\mathbf{W}_a)$ can be expressed as,

$$\mathrm{g}(\mathbf{W}_a) = c_2 - \frac{1}{2}\|\mathbf{Q}\hat{\mathbf{W}}_0^H\|_F^2, \tag{46}$$

where c_1 and c_2 are constants. Therefore, it can be noticed that optimizing $\mathbf{W}_a$ over (45) and (46) is identical. Consequently, we have shown that optimizing $\mathbf{W}_a$ over the problems (19) and (22) is equivalent, which concludes the proof.

APPENDIX III
DERIVATION OF UPPER-BOUND FUNCTION OF (22) FOR $\mathbf{W}_a$

In this appendix, we derive an upper-bound function of (22). For easy of exposition, (22) objective function is transcribed in the following

$$\mathrm{f}(\mathbf{W}_a) = ||\mathbf{W}_a\mathbf{W}_{d,0} - \hat{\mathbf{W}}_0||_F^2 + ||\mathbf{W}_a\mathbf{W}_{d,0}||_F^2. \tag{47}$$

Using the second order Taylor expansion (33), we get the following upper-bound function,

$$\begin{aligned} \mathrm{f}(\mathbf{W}_a) \leq &\beta^{-1}\|\mathbf{W}_a - \mathbf{W}_{a,0}\|_F^2 \\ &+2\Re(\mathrm{tr}(\nabla^H\mathrm{f}(\mathbf{W}_{a,0})(\mathbf{W}_a - \mathbf{W}_{a,0}))) + c \end{aligned} \tag{48}$$

where c represents a constant, and $\beta = 1/\lambda_{\max}(\mathbf{H}_{\mathrm{f}(\mathbf{W}_a)})$. As the CM constraint makes $\|\mathbf{W}_a\|_F^2 = 1$, then (48) can be simplified to

$$-2\beta^{-1}\Re(\mathrm{tr}((\mathbf{W}_{a,0} - \beta\nabla\mathrm{f}(\mathbf{W}_{a,0}))^H\mathbf{W}_a)) + c_1 \tag{49}$$

where the gradient is given by,

$$\nabla\mathrm{f}(\mathbf{W}_{a,0}) = 2\mathbf{W}_{a,0}\mathbf{W}_{d,0}\mathbf{W}_{d,0}^H - \hat{\mathbf{W}}_0\mathbf{W}_{d,0}^H \tag{50}$$

and the Hessian is $\mathbf{H}_{\mathrm{f}(\mathbf{W}_a)} = 2\mathbf{W}_{d,0}\mathbf{W}_{d,0}^H$.

REFERENCES

[1] B. Paul, A. R. Chiriyath and D. W. Bliss, "Survey of RF communications and sensing convergence research," *IEEE Access*, vol. 5, pp. 252-270, 2017.

[2] C. Sturm and W. Wiesbeck, "Waveform Design and Signal Processing Aspects for Fusion of Wireless Communications and Radar Sensing," *Proc IEEE Inst Electr Electron Eng*, vol. 99, no. 7, pp. 1236-1259, July 2011.

[3] O. B. Akan and M. Arik, "Internet of radars: sensing versus sending with joint radar-communications," *IEEE Commun. Mag.*, vol. 58, no. 9, pp. 13-19, Sept. 2020.

[4] A. Gameiro, D. Castanheira, J. Sanson and P. Monteiro, "Research challenges, trends and applications for future joint radar communications systems," *Wireless Personal Communications*, vol. 100, no. 1, pp. 81-96, March 2018.

[5] L. Leyva, D. Castanheira, A. Silva, A. Gameiro and L. Hanzo, "Cooperative Multiterminal Radar and Communication: A New Paradigm for 6G Mobile Networks," *IEEE Veh. Technol. Mag.* vol. 16, no. 4, pp. 38-47, Dec. 2021.

[6] F. Liu, C. Masouros, A. P. Petropulu, H. Griffiths and L. Hanzo, "Joint radar and communication design: applications, state-of-the-art, and the road ahead," *IEEE Trans. Commun.*, vol. 68, no. 6, pp. 3834-3862, June 2020.

[7] A. Hassanien, M. G. Amin, E. Aboutanios and B. Himed, "Dual-function radar communication systems: a solution to the spectrum congestion problem," *IEEE Signal Process. Mag.*, vol. 36, no. 5, pp. 115-126, Sept. 2019.

[8] G. Ding, Y. Jiao, J. Wang, Y. Zou, Q. Wu, Y. Yao and L. Hanzo, "Spectrum inference in cognitive radio networks: algorithms and applications," *IEEE Commun. Surveys Tuts.*, vol. 20, no. 1, pp. 150-182, 2018.

[9] L. Zheng, M. Lops, Y. C. Eldar and X. Wang, "Radar and Communication Coexistence: An Overview: A Review of Recent Methods," *IEEE Signal Process Mag*, vol. 36, no. 5, pp. 85-99, Sept. 2019.

[10] C. Chen, H. Song, Q. Li, F. Meneghello, F. Restuccia and C. Cordeiro, "Wi-Fi Sensing Based on IEEE 802.11bf," *IEEE Commun. Mag.*, vol. 61, no. 1, pp. 121-127, January 2023

[11] H. Tataria, M. Shafi, A. F. Molisch, M. Dohler, H. Sjöland and F. Tufvesson, "6G Wireless Systems: Vision, Requirements, Challenges, Insights, and Opportunities," *Proc IEEE Inst Electr Electron Eng*, vol. 109, no. 7, pp. 1166-1199, July 2021.

[12] Z. Cheng, Z. He and B. Liao, "Hybrid Beamforming Design for OFDM Dual-Function Radar-Communication System," *IEEE J Sel Top Signal Process*, vol. 15, no. 6, pp. 1455-1467, Nov. 2021.

[13] F. Liu, C. Masouros, A. Li, H. Sun and L. Hanzo, "MU-MIMO Communications With MIMO Radar: From Co-Existence to Joint Transmission," *IEEE Trans. Wirel. Commun.*, vol. 17, no. 4, pp. 2755-2770, April 2018.

[14] X. Liu, T. Huang, N. Shlezinger, Y. Liu, J. Zhou and Y. C. Eldar, "Joint Transmit Beamforming for Multiuser MIMO Communications and MIMO Radar," *IEEE Trans. Signal Process.*, vol. 68, pp. 3929-3944, 2020.

[15] L. Chen, Z. Wang, Y. Du, Y. Chen and F. R. Yu, "Generalized Transceiver Beamforming for DFRC With MIMO Radar and MU-MIMO Communication," *IEEE J. Sel. Areas Commun.*, vol. 40, no. 6, pp. 1795-1808, June 2022.

[16] F. Liu and C. Masouros, "Hybrid Beamforming with Sub-arrayed MIMO Radar: Enabling Joint Sensing and Communication at mmWave Band," *2019 IEEE International Conference on Acoustics, Speech and Signal Processing (ICASSP)*, Brighton, UK, 2019.

[17] Zeng, J., Liao, B. "Transmit and receive hybrid beamforming design for OFDM dual-function radar-communication systems," *EURASIP J. Adv. Signal Process.*, March 2023.

[18] X. Wang, Z. Fei, J. A. Zhang and J. Xu, "Partially-Connected Hybrid Beamforming Design for Integrated Sensing and Communication Systems," *IEEE Trans. Commun.*, vol. 70, no. 10, pp. 6648-6660, Oct. 2022.

[19] C. Qi, W. Ci, J. Zhang and X. You, "Hybrid Beamforming for Millimeter Wave MIMO Integrated Sensing and Communications," *IEEE Commun. Lett.*, vol. 26, no. 5, pp. 1136-1140, May 2022.

[20] Cheng, Ziyang, Linlong Wu, Bowen Wang, Bhavani Shankar, Bin Liao, and Björn Ottersten, "Hybrid Beamforming in mmWave Dual-Function Radar-Communication Systems: Models, Technologies, and Challenges." arXiv preprint arXiv:2209.04656 (2022).

[21] M. Biguesh and A. B. Gershman, "Training-based MIMO channel estimation: a study of estimator tradeoffs and optimal training signals," *IEEE Trans. Signal Process.*, vol. 54, no. 3, pp. 884-893, March 2006.

[22] Q. Shi, M. Razaviyayn, Z. -Q. Luo and C. He, "An Iteratively Weighted MMSE Approach to Distributed Sum-Utility Maximization for a MIMO Interfering Broadcast Channel," *IEEE Trans. Signal Process.*, vol. 59, no. 9, pp. 4331-4340, Sept. 2011

[23] O. Ayach, S. Rajagopal, S. Surra, Z. Piand and R. Heath, "Spatially Sparse Precoding in millimeter wave MIMO systems," *IEEE Trans. Wireless Commun.*, Vol. 13, no. 3, p. 1499–1513, Mar. 2014.

[24] D. Wilcox and M. Sellathurai, "On MIMO radar subarrayed transmit beamforming," *IEEE Trans. Signal Process.*,vol. 60, no. 4, pp. 2076–2081, Apr 2012.

[25] S. S. Christensen, R. Agarwal, E. De Carvalho and J. M. Cioffi, "Weighted sum-rate maximization using weighted MMSE for MIMO-BC beamforming design," *IEEE Trans. Wirel. Commun.*, vol. 7, no. 12, pp. 4792-4799, December 2008.

[26] Y. Sun, P. Babu and D. P. Palomar, "Majorization-Minimization Algorithms in Signal Processing, Communications, and Machine Learning," *IEEE Trans. Signal Process.*, vol. 65, no. 3, pp. 794-816, 1 Feb.1, 2017.